Determining Functional Connectivity using fMRI Data with Diffusion-Based Anatomical Weighting

F. DuBois Bowman[*], **Lijun Zhang**, **Gordana Derado**, and **Shuo Chen**
Department of Biostatistics and Bioinformatics, Center for Biomedical Imaging Statistics, Rollins School of Public Health, Emory University, Atlanta, GA

Abstract

There is strong interest in investigating both functional connectivity (FC) using functional magnetic resonance imaging (fMRI) and structural connectivity (SC) using diffusion tensor imaging (DTI). There is also emerging evidence of correspondence between functional and structural pathways within many networks (Skudlarski et al., 2008; van den Heuvel et al., 2009; Greicius, et al., 2009), although some regions without SC exhibit strong FC (Honey et al., 2009). These findings suggest that FC may be mediated by (direct or indirect) anatomical connections, offering an opportunity to supplement fMRI data with DTI data when determining FC. We develop a novel statistical method for determining FC, called anatomically-weighted FC (awFC), which combines fMRI and DTI data. Our awFC approach implements a hierarchical clustering algorithm that establishes neural processing networks using a new distance measure consisting of two components, a primary functional component that captures correlations between fMRI signals from different regions and a secondary anatomical weight reflecting probabilities of SC. The awFC approach defaults to conventional unweighted clustering for specific parameter settings. We optimize awFC parameters using a strictly functional criterion, therefore our approach will generally perform at least as well as an unweighted analysis, with respect to intracluster coherence or autocorrelation. AwFC also yields more informative results since it provides structural properties associated with identified functional networks. We apply awFC to two fMRI data sets: resting-state data from 6 healthy subjects and data from 17 subjects performing an auditory task. In these examples, awFC leads to more highly autocorrelated networks than a conventional analysis. We also conduct a simulation study, which demonstrates accurate performance of awFC and confirms that awFC generally yields comparable, if not superior, accuracy relative to a standard approach.

Keywords

functional connectivity; structural connectivity; clustering; resting-state networks; auditory processing; DTI; fMRI

Address correspondence to: Dr. F. DuBois Bowman, Department of Biostatistics and Bioinformatics, Rollins School of Public Health, Emory University, 1518 Clifton Road, N.E. Atlanta, GA 30322, Phone: (404) 712-9643, Fax: (404) 727-1370, dbowma3@emory.edu.

Publisher's Disclaimer: This is a PDF file of an unedited manuscript that has been accepted for publication. As a service to our customers we are providing this early version of the manuscript. The manuscript will undergo copyediting, typesetting, and review of the resulting proof before it is published in its final citable form. Please note that during the production process errors may be discovered which could affect the content, and all legal disclaimers that apply to the journal pertain.

1. INTRODUCTION

Resting-state and task-related brain activity reflect functional connectivity (FC) or associations between the localized neural processing from different regions. An important objective of many neuroimaging statistical analyses is to evaluate FC by spatially organizing the brain into distributed systems on the basis of the temporal coherence between spatially remote neurophysiologic events (Friston et al. 1993). Such systems consist of brain regions that exhibit relatively high correlations (or homogeneous temporal signals) within components and low correlations between the components.

There is a putative relationship between FC associations in neural processing and the brain's underlying structural circuitry. Thus, diffusion tensor imaging (DTI), which enables the reconstruction and probabilistic quantification of major fiber tracts in the brain, provides structural connectivity (SC) information that may improve our understanding of FC. Joint investigations involving fMRI and DTI often proceed either by examining the correspondence between SC and voxel-wise analysis of functional neuroimaging data or by using SC to guide region selection for FC evaluation (Rykhlevskaia et al., 2008). Such studies have demonstrated that FC is often accompanied by strong SC, e.g. in the default mode network (DMN) (Skudlarski et al., 2008; van den Heuvel et al., 2009; Greicius, et al., 2009). Also, Morgan et al. (2009) suggest that FC is supported by SC along the language pathways. However, FC has also been reported between regions that do not exhibit accompanying evidence of direct structural links (Honey et al., 2009; Greicius, et al., 2009). These functional associations may arise from indirect structural pathways, from structural pathways that are not easily detected by DTI, or as a result of spurious correlations in neural activity. As the association between brain structure and function is further revealed by studies combining both modalities, an important next step is to develop unified statistical frameworks that incorporate both sources of information simultaneously while coping with the complexities of the relationship, e.g. since the absence of SC does not preclude the possibility of FC. Such multimodality approaches would leverage the relationship between brain structure and function and lead to more robust and informative analyses.

Cluster analysis is well-suited for identifying functionally related brain regions. Clustering is a long-standing statistical method with numerous applications in functional neuroimaging, including applications of the *K*-means algorithm (Balslev et al., 2002; Goutte et al., 2001), fuzzy clustering (Baumgartner et al., 2000; Fadili et al., 2001), and hierarchical clustering procedures (Bowman et al., 2004; Bowman and Patel, 2004; Cordes et al., 2002; Stanberry et al., 2003). Clustering based on blood oxygen-level dependent (BOLD) functional magnetic resonance imaging (fMRI) relies on measures of dissimilarity between the temporal BOLD signals from different brain locations. Typical dissimilarity measures include Euclidean distance, Mahalanobis distance, and one minus the (partial) correlation coefficient. A notable shortcoming of these metrics in light of recent discoveries of the correspondence between FC and SC, however, is that they ignore information regarding SC between brain regions. Considering both brain activity and the existence of anatomical links between brain regions would provide a more reliable and informative approach to identify neural processing networks.

We propose a new statistical technique, called anatomically-weighted FC (awFC), that combines fMRI and DTI data to help describe the functional organization within the human brain. We present a novel distance that measures the functional dissimilarity between brain regions, while incorporating supplemental information about the probability of SC between the regions. Our awFC technique provides flexibility to alter the level of anatomical weighting (via a model parameter) and to specify the number of neural processing networks (clusters). We optimize these quantities empirically using a strictly functional criterion, so

by incorporating neuroanatomic information, our approach will generally perform at least as well as a conventional unweighted (fMRI only) analysis, with respect to intracluster coherence or autocorrelation. Moreover, awFC yields more informative results since it provides structural properties associated with identified functional networks. We illustrate the use of our awFC technique by applying it to resting-state fMRI data from a group of healthy subjects and to fMRI data acquired during an auditory task.

2. EXPERIMENTAL DATA

We consider both resting-state and task-based fMRI data to illustrate our awFC approach.

2.1 Resting-state fMRI Data

We use DTI and resting-state fMRI data from 6 healthy female subjects. The data were collected on a 3T Siemens scanner and include a series of 210 fMRI scans with TR=2 sec, 20 slices, and $3.4 \times 3.4 \times 4$ mm^3 voxel resolution. The functional runs were collected with a Z-saga sequence to avoid orbitofrontal signal ablation. fMRI data were preprocessed using FEAT (FMRI Expert Analysis Tool), which is part of FSL (FMRIB's Software Library, www.fmrib.ox.ac.uk/fsl). The following preprocessing steps were applied: motion correction using MCFLIRT (Jenkinson et. al., 2002), slice-timing correction, non-brain removal using BET (Smith, 2002), spatial smoothing using a Gaussian kernel of 5mm FWHM, mean intensity normalization of the volume at each time point, and high-pass temporal filtering. DTI data were acquired using a diffusion-weighted single-shot spin echo EPI sequence on a 3T Siemens Trio system. A dual spin echo technique was employed to minimize the geometric distortion induced by Eddy currents. Twelve directions were applied with the parameters: TR=2660ms, TE=86 ms, FOV=22 cm×22 cm, slice thickness =2.5 mm, slice gap=0 mm, number of slices=19, b=0, 1000s/mm2, and 12 averages. Images (128×96 matrix size) were acquired in the axial orientation.

We generate summaries of the fMRI data over 86 regions for each subject, with regions defined according to the Automated Anatomical Labeling (AAL) system (Tzourio-Mazoyer et al., 2002). To obtain the fMRI regional summaries, we first transform the voxel-level data to the frequency domain using the fast Fourier transform, average the power spectral density estimates across subjects, and apply a singular value decomposition (SVD) for each region separately to obtain the dominant frequency pattern in the region. It is beneficial to consider frequency characteristics present in the data, rather than simply averaging the data in the time-domain. At resting-state, subjects are not performing a common explicit task at each scan, so averaging across subjects in the time domain is not desirable. Next, we identify the voxel that exhibits frequency characteristics most closely resembling the regional summary and select the 150 most proximal gray matter voxels to this regional representative, ensuring that all of the selected voxels fall within the AAL region. These voxels generally exhibit coherent temporal patterns that are representative of the entire region. To summarize over the selected voxels, producing a single time series for each region and for each subject, we apply a second SVD to the time-domain data. We scale each regional time series by its ℓ^2-norm to adjust for differences in variability across regions and subjects. Since singular vectors are unique up to multiplication by a unit phase factor, we compare the singular vector to the subregion mean signal to ensure that the selected signal represents the region correctly, and we apply a sign change to our extracted signal, if necessary.

The final summaries for each subject can be viewed as a TxR matrix, where T is the number of scans and R is the number of regions (R=86 in the resting-state fMRI data) (see Figure 1a). We evaluate our final selections to ensure both that the time series is representative of the subregion and that the subregion is reasonably homogenous. For these assessments, we compute the ratio of the largest eigenvalue to the sum of the eigenvalues for both SVDs

applied to the resting-state data. For each region, the targeted power spectrum explains over 95% of the variation in the entire region. For our resting-state data, the selected time series representing the small subregions explain on average 64% of the variability, averaged across all subjects and brain regions, reflecting at least moderately coherent subregions. We restrict the percent variability explained by the first temporal profile to be greater than 40% for all subjects and for the mean across subjects to be greater than 60%. If these criteria are not met, then we choose a second voxel based on the second singular value/vector and repeat the aforementioned steps.

We perform probabilistic diffusion tensor tractography (DTT) using FDT (FMRIB's Diffusion Toolbox), which implements the approach of Behrens et al. (2003, 2007) to obtain probabilities of SC between each pair of brain regions. We define sub-regions for DTT that are centered in white matter proximal to the fMRI-based subregions. Although we restrict the seed and target regions in the DTT algorithm to white matter, the connecting streams are allowed to pass through gray matter. The FSL probabilistic DTT algorithm initially yields voxel-level counts (for the seed region) indicating the likelihood of a fiber tract extending from the voxel in a seed region to (or through) the target region (Behrens et al. (2003, 2007)). To capture strong connectivity between pairs of regions, we ordered the voxel-level counts and select the 90th percentile from the ordered counts and then appropriately divide the counts by the maximum number of streams used in the FSL DTT algorithm to form probabilities of connection. We impose symmetry by calculating the maximum of the two directional probabilities for each pair of regions. The regional summaries yield more reliable and robust measures of SC between regions, given the inherent subject-to-subject variability in voxel-to-voxel fiber tracts and functional associations.

2.2 Auditory Task

We also consider DTI data and fMRI data acquired while subjects performed an auditory attention task. Data were collected on a 3.0T Siemens Trio scanner for 17 healthy female subjects. There are three fMRI runs with 162 echo-planar images collected with TR = 2 sec, TE = 29 ms, flip angle = 75°, FOV = 240mm, matrix size = 64×64, and 33 contiguous sagittal 3.5mm thick slices with a gap of 1.05mm to cover the whole brain (voxel resolution: $3.75 \times 3.75 \times 4.55$). We eliminate the first image of each run to mitigate equilibrium effects, leaving a total of 483 scans for each subject. During the entire session, subjects fixate on a white visual cross on a black background. For the task, subjects hear an auditory tone (cue, 2000Hz) in one ear and then subsequently hear another tone (target, 1000Hz) in either ear. *Valid* trials are those in which both the cue and target tones occur in the same ear; otherwise, the trial is labeled *invalid*. There are a total of 84 valid and 84 invalid trials across three runs, and there is a 50% chance of either occurring. Subjects were instructed to click a button, either with their right index finger, if the target sounds in the left earphone, or with their right middle finger, if occurring in right earphone. The study had a broad set of objectives (not described here, see Mayer et al. (2009)). Although the study was not designed to isolate the motor, visual, and auditory signals, since all were present in the scans obtained during a task response, we apply the awFC procedure to these data. We consider scans 4–6 seconds from each target onset in the valid trials occurring in left ear, resulting in 84 scans for each subject in our analyses.

Two DTI scans with b = 800 s/mm^2 and 30 diffusion gradients were acquired using a twice-refocused spin echo sequence to reduce the effects of eddy currents and artifacts associated with head movement and to allow increased time for diffusion sensitizing gradients. Also, five sets of gradients were applied with each set containing a single b = 0 s/mm^2 followed by six b = 800 s/mm^2 directions to cover the sphere uniformly [72 interleaved slices; TE = 84 ms; TR = 9 s; flip angle = 90° ; slice thickness = 2.0 mm; FOV = 256×256 mm; matrix size = 128×128; voxel resolution = $2 \times 2 \times 2$ mm^3] (Ling et al., 2012).

We select localized subregions within each AAL region that appear to be more engaged during the auditory attention task than other areas within the region. Specifically, we identify the most engaged voxel location by considering the magnitude of activity (regardless of direction) standardized by the standard error for each contrast across subjects. Then we build a small subregion consisting of the 150 nearest voxels to the selected center, ensuring that all of the voxels fall within a single AAL region. The subregion size of 150 voxels corresponds roughly to a sphere with a 6mm radius surrounding the most active voxel, although we do not strictly require a spherical shape. We obtain BOLD fMRI summaries for each subregion by applying an SVD to extract the dominant temporal pattern (first right singular vector) with the highest associated singular value. Since singular vectors are unique up to multiplication by a unit phase factor, we compare the singular vector to the subregion mean signal to ensure that the selected signal represents the region correctly, and we apply a sign change to our extracted signal, if necessary. To evaluate the final selection of subregions, we compute the ratio of the largest eigenvalue to the sum of the eigenvalues. For auditory processing data, the selected time series explain on average 71% of the variability, averaged across all subjects and brain regions, reflecting at least moderately high coherence within subregions. We also apply DTT to the DTI data to obtain probabilities of SC between each pair of selected subregions. To reduce DTI/DTT noise, we analyze both DTI scans and average the resulting SC probabilities. Generally, there is close agreement between the two calculated SC probabilities.

2.3 Registration

We first register each subject's fMRI data to standard Montreal Neurological Institute (MNI) space. Next, we select fMRI subregions (as described previously) in standard space, which fall largely in gray matter (exclusively in gray matter for the resting-state data). These functional subregions are used to define the fMRI profiles that are input into our analysis. For the DTI data, we begin by registering a standard MNI space, skull-stripped, T1 image to each subject's Eddy corrected, brain extracted DTI image and retaining the resulting transformation matrix. For the auditory data, we select the DTI space of the first scan and register the second DTI scan to the first one. Then, in standard space, we perform white matter segmentation on a skull-stripped T1 image, we select a collection of white matter voxels that are most proximal to each selected functional subregion, and then we apply the previously obtained transformation matrix to shift these white-matter subregions to each individual's DTI space. Finally, we perform DTT using these white matter subregions in each subject's original DTI space and obtain probabilities of SC between all pairs of regions. One important property of our registration procedure is that FSL functions to estimate diffusion parameters at each voxel (BEDPOSTX) and to perform probabilistic tractography (PROBTRACKX) on each white-matter seed region both always take place in each subject's diffusion space.

3. METHODS

We propose an awFC method that combines fMRI and DTI data to explore either resting-state or task-related FC networks. Our new approach is based on cluster analysis with a novel distance measure that includes weights reflecting the evidence for underlying SC to supplement the fMRI data. In what follows, we describe the combined function-structure dissimilarity measure used in our awFC technique and then provide additional details about the functional and structural components. Figure 1 gives a schematic overview of the procedure.

Anatomically-Weighted Functional Distance

We propose a novel distance measure that combines both functional and structural information. Specifically, we propose the following anatomically-weighted distance:

$$d_{ij} = \left(1 - \frac{\pi_{ij}}{\lambda}\right) f_{ij} \qquad (1)$$

where $\pi_{ij} \in [0,1)$ is the DTT-based probability of SC between regions i and j, $\lambda \in [1, \infty) = \Lambda$ is an unknown parameter that potentially attenuates the anatomical weighting, and f_{ij} is the functional dissimilarity (distance) between the fMRI profiles and is inversely related to FC strength. Figure 1(e) displays our new anatomically weighted distance matrix, which is constructed from our resting-state fMRI data. The distance matrix reflects modest shrinkage of the functional distances toward zero, with the extent of shrinkage for a particular region pair being determined by the corresponding strength of SC.

Hierarchical clustering uses dissimilarity measures, rather than similarities, as criteria for joining regions into networks, so smaller values of d_{ij} in equation (1) prompt regions i and j to merge into the same network. Standard clustering approaches for functional neuroimaging data only consider the functional term f_{ij}. By including the first factor $w_{ij} = (1 - \pi_{ij}/\lambda)$, which is inversely related to the strength of SC, our awFC technique is more likely to form networks consisting of regions exhibiting highly correlated brain activity when there is corresponding information revealing strong SC. Importantly, since SC is not a necessary condition for FC, our awFC method may still detect FC in the absence of SC, i.e. when $\pi_{ij} = 0$, as our approach defaults to standard procedures considering only f_{ij}. This property of our anatomically weighted distance preserves functional-structural relationships revealed by Greicius et al. (2009) and Honey et al. (2009) and helps to counter false negative DTT results. Also, since SC is not a sufficient condition for FC, i.e. structural links may be present without FC exhibited during a particular task (or at rest), we include a parameter λ that attenuates the role of SC so that regions with high probabilities of SC do not necessarily belong to the same network without accompanying evidence of FC. The parameter λ may also protect against the impact of false positive SC results (e.g. when λ is large). Below, we provide a strategy for empirically optimizing λ from the data and elaborate on how to obtain π_{ij} and f_{ij}.

3.1 Functional Distances

To determine the functional dissimilarity between BOLD fMRI profiles in regions i and j, we compute functional distances at lag-u using one minus the correlation (or partial correlation) between the corresponding time series, i.e.

$$f_{ij} = \min_{u \in U} f_{ij}(u) = \min_{u \in U} \left\{ 1 - \frac{\sum_{t=1}^{T-u} [y_i(t+u) - \bar{y}_i][y_j(t) - \bar{y}_j]}{\widehat{\sigma}_i \widehat{\sigma}_j} \right\}, \qquad (2)$$

where $y_i(t)$ is the fMRI-based regional summary of brain activity in region i at time t, $\hat{\sigma}_i$ and $\hat{\sigma}_j$ represent the sample standard deviations of $\mathbf{y}_i$ and $\mathbf{y}_j$, respectively, and $\bar{y}_i$ and $\bar{y}_j$ represent the sample means of $\mathbf{y}_i$ and $\mathbf{y}_j$, respectively. For ease of interpretation, we restrict our attention to positive correlations, although one could easily retain the negative correlations in the analysis, possibly making the small adjustment of remapping correlations in the range [−1 1] to [0 1] using a suitable transformation. Interpretations may be more difficult, however, when the chief interest is in detecting clusters of negatively correlated brain

regions. Given potential differences in the hemodynamic responses to task-related or resting-state neuronal activity in different regions, we evaluate the functional distances at several lags u in [−3, 3] and obtain the minimum lag-u distance. Thus, the functional distance matrix (see Figure 1(c)) with elements f_{ij} gives a measure of how uncorrelated the resting-state fMRI-based regional profiles (Figure 1(a)) are between every pair of brain regions.

3.2 Structural Distances

The structural dissimilarity is interpretable as the weakness of SC between pairs of regions. To determine the structural dissimilarity, we first apply probabilistic DTT as previously described to compute region-to-region probabilities of SC π_{ij}. We allow for indirect (second-order) SC between regions by defining $\pi_{ij} = \max[\pi_{ij}, \max_m (\pi_{im}\pi_{mj})]$. Since the quantities π_{ij} represent the strengths of structural connections between pairs of regions i and j, we compute the structural distances (*weaknesses* of SC) using $w_{ij}=(1-\pi_{ij}/\lambda)$, where λ is an unknown parameter that potentially attenuates the impact of the structural data. Larger values of λ result in less anatomical weighting. The quantities w_{ij} are in the interval [0, 1]. Figure 1(d) shows the structural distance matrix with elements w_{ij}, where $\lambda=1$, obtained from DTI data acquired in the resting-state fMRI study.

We obtain π_{ij} using probabilistic DTT implemented in FSL (Behrens et al., 2007), but other approaches are also available (e.g. Lazar and Alexander, 2005; Parker et al., 2003). The FSL algorithm casts streams from a seed region and applies stopping rules for the streams based on direction angles and fractional anisotropy. Conceptually, the FSL DTT algorithm may yield biased tractography relating to the physical (geometric) distances between brain locations, since neighboring voxels may have inflated SC probabilities. We perform our analysis at a region level, where all region pairs are separated by more than 17.4 mm, which based on simulations (not shown), leads to negligible bias due to distance-related false positive connections. We also employ a Poisson regression-based statistical adjustment that yields measures of SC adjusted for the physical distances between region locations. Specifically, we apply a model that assumes that the number of DTT streams S_{ij} connecting regions i and j follows a Poisson distribution with the mean $\mu(S_{ij}|g_{ij})$ dependent on the physical distance g_{ij} between these regions, i.e. $S_{ij}|g_{ij} \sim \text{Poi}(\mu(S_{ij}|g_{ij}))$. Therefore, we estimate and subsequently adjust for the association between the physical distances and the DTT counts using the effect a_1 in the log-linear model $\log(\mu(S_{ij}|g_{ij}) = a_0 + a_1 g_{ij}$. Henceforth, assume that each π_{ij} is adjusted for physical distance to reduce the potential impact of false structural connections on our awFC method.

3.3 Clustering

We use the average linkage (AL) method to cluster data (group- or individual-level), specifically applied to the new anatomically-weighted distance measure. We prefer AL over other clustering procedures because hierarchical methods do not involve stochastic initialization, making it possible to implement a replicable optimization procedure, AL yields distances that satisfy properties of a proper distance metric for the fMRI and DTI data that we consider, and AL typically performs well in neuroimaging applications (Bowman et al., 2004). AL begins with each region representing its own cluster. At each iteration, two clusters merge if (on average) the pair has the smallest distance d_{ij}, and the iterative process ceases when only a single cluster remains. We then optimize the number of clusters G and the parameter λ as described in the next subsection.

3.4 Optimization

Our awFC technique establishes G neural processing networks from the total number of brain regions, R, and applies the anatomical weighting attenuation parameter λ. These

quantities are unknown, so we propose an empirical optimization procedure for obtaining them. We define an objective function, which depends on FC properties of the data, to simultaneously optimize the number of clusters G and the attenuation parameter λ. By determining λ based only on the functional data, awFC generally performs at least as well as standard clustering that considers only fMRI data, e.g. with respect to intracluster coherence or autocorrelation. If the inclusion of structural data does not improve FC properties, e.g. by introducing noise, then our method tends to default to the standard procedure by optimizing λ such that $(\pi_{ij}/\lambda) \approx 0$ for all region pairs.

Our objective function assesses the relative strength of FC exhibited by a set of clustering solutions. Let $FCwi$ denote the strength of FC within identified networks. Specifically, we calculate $FCwi$ as the average of the correlations (each maximized over lag-u, e.g. u in $[-3,3]$) for all within-cluster region pairs, and similarly $FCtot$ is the average FC over all region pairs in the entire brain. We regard a good clustering solution as one whose intracluster regions exhibit relatively high correlations between the associated fMRI time series. Thus, we define the following objective function to optimize the clustering solution with respect to G and λ:

$$h(\lambda, G) = \log\left(\frac{FCwi}{FCtot}\right). \tag{3}$$

Larger values of $h(\lambda, G)$ reveal a better clustering solution. As the number of clusters G increases, $h(\lambda, G)$ will generally reflect a better clustering solution. So we calculate $\Delta(\lambda, G) = h(\lambda, G) - h(\lambda, G-1)$, which compares the improvements in fit from $G-1$ to G clusters for a given value of λ, following a similar strategy to the pseudo-T^2 stopping criterion for hierarchical clustering [Duda and Hart, 1973; Bowman et al., 2004]. Let $\Delta(\lambda)$ and $\Delta(G)$ represent marginal forms of the objective function obtained by summing over the omitted argument. For a single subject, we optimize λ as $\lambda_{opt} = \arg\max_{\lambda \in \Lambda}\{\Delta(\lambda)\}$. More often, we are interested in conducting group analyses, and we provide details in the next subsection for optimizing λ in this case. We select the optimal G from $\Delta(G)$ as the number of clusters beyond which there is relatively little improvement in fit. We implement our procedure in practice by optimizing over a relatively fine grid of points $\{(\lambda, G) \mid G = 2, \ldots, R \text{ and } \lambda \in \Lambda\}$.

3.5 Group Analysis

We formulate our procedure so that anatomically weighted clustering is performed for each subject separately, yet we are able to construct group cluster assignments based on the subject-specific networks. We define group FC between two regions based on consistent replication of FC across subjects. Specifically, to construct group networks, we begin by determining the probability that each region pair falls within the same network, simply estimated by the proportion of subjects for which this holds. We then threshold these probabilities at a specified level to declare within-network and cross-network region pairs, for all pairs of brain regions, which can be viewed as a connectivity matrix. We are then able to reconstruct group-level FC networks, reflecting highly probable networks (across subjects). To ensure consistent interpretation of the networks across subjects, we restrict the attenuation parameter for anatomical weighting to be equal for all subjects. Specifically, we select λ for group analyses as $\lambda_{opt} = \arg\max_{\lambda \in \Lambda}\left\{\sum_{i=1}^{n}\Delta_i^*(\lambda)\right\}$, where $\Delta_i^*(\lambda) = \Delta_i(\lambda)/\max_{\lambda \in \Lambda}(\Delta_i(\lambda))$. Also at the group level, G is optimized separately for each subject.

3.6 Network Validation

Clustering algorithms assign every brain region to a cluster. Following construction of the group networks, we examine each cluster to distinguish between region pairs that possess *true* functional relationships and those that do not. Specifically, we test the statistical significance of the correlations between all within-network region pairs via the hypotheses:

$$H_0:\rho_{ij}=\rho_0 \quad \text{vs.} \quad H_1:\rho_{ij}>\rho_0, \tag{4}$$

for all intracluster region pairs (i, j) using Mann-Whitney U tests with a Bonferonni multiple testing adjustment for the number of tests performed within each network. Setting $\rho_0=0$ may detect the presence of minimal levels of FC, but given *background* correlations inherent in functional neuroimaging data that are not associated with defined network structure, we suggest testing at stronger levels of FC by specifying values of at least $\rho_0 = 0.10$. We use $\rho_0 = 0.25$ in our upcoming data examples, and we connect regions with bars to graphically depict region pairs having statistically significant correlations. These validation procedures may allow us to identify one or more noise regions that are assigned to an otherwise homogeneous cluster or to identify several noise regions assigned to a single cluster. One could alternatively consider adding a pruning procedure upon the completion of our awFC method, which would evaluate the potential removal of each region (individually) in a cluster and establish a criteria for removal, e.g. if the removal leads to marked improvement in the within cluster coherence.

4. DATA EXAMPLE AND RESULTS

We apply our anatomically-weighted clustering procedure to the previously described resting-state fMRI and DTI data and the task-based fMRI study involving auditory processing.

4.1 Resting-state fMRI Study

Our analysis seeks to determine FC by organizing the resting-state activity throughout the brain within component subsystems or networks. We also describe properties of within-network brain activity patterns and between network associations.

We perform subject-specific awFC analyses for a range of values of $\lambda \in [1,\infty)$ and for varying G (the number of clusters). Figure 2(a) displays $\sum_{i=1}^{n} \Delta_i^*(\lambda)$ versus various values of λ, and Figure 2(b) shows $\Delta(G)$ versus G for subject 1 in the resting-state fMRI data. To ensure consistent interpretations of FC across subjects, we use constant SC, determined to be here. For subject 1, $G=9$ is a reasonable selection for the number of clusters since there is limited improvement revealed by $\Delta(\lambda,G)$ beyond this point. Note that the horizontal reference line in Figure 2(b) is arbitrarily selected to correspond to the 75th percentile. The subject-specific networks generally contain brain regions with highly synchronous fMRI profiles.

Figure 3 presents three selected group-level clusters from the awFC procedure applied to our resting-state fMRI data from a total of 16 clusters. We construct group networks based on region pairs that exhibit FC (within the same network) in at least 4 of the 6 subjects. Several brain regions previously reported among resting-state networks (RSNs) (Buckner et al., 2008; Fox et al., 2005) are largely distributed across three clusters in our analysis. Cluster 1 captures a triad of (a) medial prefrontal cortex, namely left superior medial frontal gyrus (BA 10), (b) bilateral posterior cingulate, right caudal middle cingulate, and the left ventral precuneus (BA 23/4), and (c) the left inferior parietal region and angular gyrus (BA 48/40/5). This network points to the integration of (a) executive functioning, (b) experiential

self-reflection, autobiographical memories, or self-referential decision-making (Cavanna and Trimble, 2006; Fink et al., 1996; Johnson et al., 2006; Maddock, 1999), and (c) the perception and interpretation of sensory information. Cluster 2 identifies a memory-related network in the medial temporal lobe that includes the hippocampus, right parahippocampus, and right amygdala (BA 28/34/35). Cluster 3 represents a visual network that includes the left middle occipital gyrus, left and right cuneus and lingual gyrus, and left and right calcarine sulcus (BA 17/18/19) and that extends to a posterior region of the right precuneus (BA 25). This network is highly consistent with a resting-state visual network identified by Wang et al. (2008).

The functional coherence of each network is relatively high. The distribution of pairwise correlations for each network is skewed, zero-inflated, and quite disperse. Therefore, we report the minimum, first quartile, median, third quartile, and maximum, reflecting the central tendency, dispersion, and range of the distributions. The five-number summary for cluster 1 is [0, 0.20, 0.42, 0.63, 0.93], for cluster 2 is [0, 0.16, 0.41, 0.56, 0.84], and for cluster 3 is [0, 0.16, 0.46, 0.66, 0.95]. The median correlation between all region pairs in each of these networks exceeds 0.4, with maximum correlations exceeding 0.8.

Several RSN regions have been shown to exhibit strong SC (Skudlarski et. al., 2008; van den Heuvel et al., 2009; Greicius, et al., 2009). In our analysis, the distribution of the pairwise SC for each network generally has density concentrated primarily near zero (unconnected) and secondarily near one (connected), with much less density distributed across the intermediate values. To summarize the within-network strength of SC, we calculate the proportion of region pairs with SC probabilities exceeding 0.5, interpretable as the proportion of structurally connected region pairs. The DTT probabilities indicate that 22.62% of the region pairs in cluster 1 are structurally connected, 36.11% of the region pairs in cluster 2 are structurally linked, and white-matter fiber tracts connect 22.62% of the region pairs in cluster 3.

The complete set of brain networks identified in our analysis collectively achieves a higher degree of functional coherence and stronger SC than between-network region pairs. Figure 4(a) shows the median correlation between all within-network pairs and the median correlation for all between-network pairs for each subject. The in-network median correlations range from 0.33 to 0.54 across subjects and consistently exceed the cross-network correlations, which range from 0.06 to 0.12. The differences between the median correlations from within-network region pairs versus cross-network region pairs are all statistically significant based on Mann-Whitney U tests, with p-values less than 0.0001 for each subject.

The structural integrity of within-cluster region pairs is also consistently higher than the SC for cross-cluster region pairs for all subjects (see Figure 4(b)). The proportion of region pairs exhibiting SC is significantly higher within the set of functionally connected networks than it is for cross-network region pairs. Specifically, the proportion of structurally connected regions within the functionally connected networks ranges from 0.25 to 0.39, while these quantities range from 0.11 to 0.21 for cross-network region pairs. The differences in the proportion of structurally connected region pairs shown in Figure 4(b) are statistically significant, with p-values less than 0.0001 for each subject.

The collective set of networks identified by our awFC analysis also exhibits correlations between FC and SC for most subjects, despite the complexity of the relationship between these measures discussed previously. The correlations between FC and SC within the complete set of networks range from 0.08 to 0.26 across subjects, and these correlations are statistically significant for all but one subject. These FC-SC correlations, even when

evaluated at a global level, support our use of SC to help determine functional networks. The relationship will clearly be stronger between some region pairs and within particular networks. Our awFC method flexibly leverages this relationship in a way that neither penalizes when the correlation between structure and function is low nor assumes FC based on strong SC properties.

For comparison, we perform a conventional analysis based solely on the fMRI data, without introducing anatomical weighting. Given that the awFC procedure optimizes the attenuation parameter based solely on FC properties, it will generally perform at least as well as the standard clustering approach. To compare the global intra-network coherence between our awFC approach and conventional clustering, we evaluate the median (and mean) of the within-cluster correlations between region pairs (across all clusters and across all subjects) as well as the functional autocorrelation calculated using the average value of Moran's I across subjects (Derado et al., 2010). The awFC procedure yields a 4.7% improvement in within-network FC relative to unweighted clustering. Our awFC clustering solution yields a 14.0% improvement in functional autocorrelation, on average, relative to the standard procedure. The increased coherence present in the awFC solution reflects an advantage of our approach over the unweighted analysis for these data.

4.2 Auditory Processing fMRI Study

We consider the application of the awFC method to fMRI data collected while subjects performed an auditory processing task, which additionally involves visual and motor processes (Mayer et. al., 2009). The group-level awFC results for the task data appear in Figure 5. Here, we define group-level FC between regions by at least 12 of the 17 subjects (70.6%) exhibiting FC, i.e. FC is consistently replicated across subjects. Our analysis identifies a total of 18 networks, and 5 of these largely capture motor, visual, and auditory components of the task. Clusters 1 and 2 contain several known motor regions including primary and supplementary motor regions (BA 4/6) as well as subcortical motor regions in the basal ganglia (BA 48). Clusters 3 and 4 contain the primary visual cortex, secondary visual cortex, and visual association cortex (BA 17/18/19) and extend to a posterior region of the right precuneus (BA 7). Note that the visual cluster 3 exhibits broad similarity to the visual network identified during the awFC analysis of the resting-state data, and subjects performed visual fixation in both studies. Cluster 5 contains primary and secondary auditory cortex (BA 42/48/22), including the right superior temporal gyrus, Heschl gyrus, and supramarginal gyrus.

The networks identified by our analysis contain brain regions with very highly coherent neural activity. The median correlations between fMRI profiles for all of the region pairs (across all subjects) in the motor network clusters are 0.77 (cluster 1) and 0.73 (cluster 2). The median correlations for clusters in the visual network are 0.75 (cluster 3) and 0.66 (cluster 4). The median correlation for the identified auditory network is 0.74. Our awFC method yields more functionally coherent networks than standard unweighted clustering for these data as revealed by a 9.2% increase in Moran's I. There is individual variability in the clustering solutions, both in the original subject-specific networks and the degree of within-cluster coherence corresponding to the group cluster maps. The subject-specific networks generally contain brain regions with highly synchronous fMRI profiles. For the auditory data, the individual subjects conform closely to the group solution. We display the regional profiles corresponding to the *group* clustering solution for three selected subjects (see Figure S1 in the online Supplementary Materials). Examining subject 2, for example, the brain regions in all clusters reveal very strong positive correlations. Estimates of the correlations between fMRI regional profiles are 0.74 and 0.8 in the motor network (clusters 1–2, respectively), 0.83 and 0.69 in the visual network (clusters 3 and 4), and 0.83 in the auditory network (cluster 5).

Relatively few region pairs in the motor network exhibit SC, defined here as having DTT-based SC probabilities exceeding 0.5. Specifically, fewer than 3% of the region pairs exhibit SC in cluster 1 and 6.86% in cluster 2. On the other hand, the visual networks have relatively strong structural circuitry, with 42.02% of the region pairs revealing SC for cluster 3 and 40% of the region pairs in cluster 4 exhibiting SC. Cluster 5, the auditory cluster, exhibits moderate structural connectivity, with 16.53% of the region pairs revealing SC.

Globally, the in-network correlations far exceed the correlations for cross-network region pairs. The in-network median correlations range from 0.43 to 0.77 across subjects (see Figure 6(a) (red)), whereas the cross-network median correlations range from 0.18 to 0.47 (see Figure 6(a) (blue)). The differences between the median correlations from within-network region pairs versus cross-network region pairs are all highly statistically significant based on Mann-Whitney U tests, with p-values less than 0.0001 for each subject. The structural integrity of within-cluster region pairs is higher than the SC for cross-cluster region pairs for all subjects (see Figure 6(b)). The differences in the proportion of structurally connected region pairs shown in Figure 6(b) are statistically significant for 16 of the 17 subjects, with p-values less than 0.0059 (corresponding to a familywise error rate of $\alpha = 0.10$).

Small to moderate correlations between FC and SC exist within the complete set of networks, ranging from 0.16 to 0.32 across subjects. These FC-SC correlations are statistically significant for 16 of the 17 subjects, with p-values less than 0.006 (p-value=0.05 for the remaining subject, which is nonsignificant when adjusting for multiple comparisons). These significant FC-SC correlations support our use of SC to help determine functional networks.

5. SIMULATION STUDY

We conduct a simulation study to examine the performance of our awFC technique. We base our simulations on the featured resting state fMRI and DTI data described earlier. The functional distances in these data roughly follow a normal distribution with different mean and variance parameters for within-network and cross-network region pairs. The DTT-based SC probabilities are well-approximated by a gamma distribution, again with separate parameters for within-network and cross-network region pairs. Moreover, the functional and structural distances exhibit correlations. Details about our simulation model appear in the Appendix. Our analysis shows that awFC generally performs well for the simulated data.

Simulation Results

Using our experimental data to define the brain networks, to set the parameter values for the selected probability distributions, and to set the optimized value of $\lambda = 7.5$, we draw 5000 simulated data sets, perform the awFC procedure on each, and evaluate the accuracy of our clustering results. We repeat the procedure to evaluate the influence of varying noise levels on the performance.

We estimate the accuracy among in-network, cross-network, and all region pairs. The results appear in Table 1. The defined (true) underlying networks consist of 483 (13.86%) within-network region pairs and 3003 (86.14%) cross-network pairs. Generally, awFC refrains from merging cross-network region pairs into the same clusters. Even when we add substantial noise, awFC performs quite well for the cross-network region pairs. Also, awFC accurately identifies 98.07% of the within-network region pairs when the variability of the simulated data equals that exhibited by the experimental data (noise level σ^2). The within-network accuracy remains high at 91.17% when we inflate the variability by a factor of two. Further masking the network structure with a noise level of $3\sigma^2$, which far exceeds what is likely to

be observed when analyzing experimental data, we note a decrease in the performance of awFC to 82.79% for in-network region pairs, but the performance is still reasonably good. The overall accuracy for awFC is quite high (exceeding 95%) for all noise levels that we consider.

We also perform corresponding unweighted cluster analyses on the simulated data. For the simulated data, there are only moderate differences between the awFC procedure and the conventional unweighted approach, likely due to the relatively large value of the optimal attenuation parameter $\lambda=7.5$. However, the awFC procedure outperforms unweighted clustering in every case that we consider, and the differences in performance between awFC and unweighted clustering become more marked as the noise level increases.

6. DISCUSSION

We present a new procedure to determine FC by combining information derived from fMRI and DTI data. This method, which we refer to as awFC, is applicable to either resting-state or task fMRI studies. AwFC identifies a set of brain networks, where each network consists of regions that exhibit relatively similar (correlated) temporal BOLD fMRI profiles. AwFC utilizes the probabilities of structural connections between regions as supplemental criteria for establishing these functional networks. We derive a novel distance measure to combine the structural and functional associations between regions according to principles that establish an increased chance of FC between brain regions with both similar neural processing characteristics and evidence of underlying SC. However, these principles are sufficiently flexible so that they do not preclude the possibility of detecting FC between brain regions with weak or no evidence of SC, nor do they necessarily identify FC between regions with strong SC. Our awFC method yields both individual-level and group-level clustering results. After the initial data processing required to obtain detrended regional fMRI profiles and DTT estimates of region-to-region SC for each subject, our awFC technique executes very quickly in MATLAB, taking only a couple of minutes on a standard Pentium 4 desktop computer.

Our analysis is based upon defining fairly focal and coherent subregions across the entire brain, which either are representative of larger brain regions (e.g. AAL or Brodmann) or are most engaged in a particular task or set of tasks. One potential challenge to the successful definition of representative subregions is that some of the initial regions from the AAL or Brodmann parcellation are too heterogeneous. For example, a single BA may consist of two or more dominant patterns of neural activity. One remedy to address this issue is to consider further (possibly functionally defined) partitions on the AAL or BAs prior to using our methods to define subregions. One could also begin with an alternative parcellation to AAL or BAs, e.g. one proposed by Craddock et al. (2011), which could define spatially finer (and likely more homogenous) regions. These alternatives may also be implemented to improve the spatial coverage of the brain for analysis.

Our awFC analysis of the experimental resting-state fMRI and DTI data obtained from healthy subjects identifies three networks that capture several RSN regions. The three identified networks generally represent a memory-related component (hippocampus, parahippocampus, and the fusiform gyrus), a visual component (precuneus, posterior cingulate, and middle occipital region), and a network integrating executive functioning (medial prefrontal cortical), self-referential decision-making (the middle cingulate), and the perception and interpretation of sensory information (the left and right inferior parietal regions). Our awFC analysis of the task fMRI data reveals networks associated with auditory, visual, and motor processing.

The global FC across all networks for the task data is generally higher than for the resting state data, both within and across networks. This finding seems reasonable given the focused engagement in a particular (auditory) task, relative to subjects left to think for themselves during the resting state scans. The SC supporting the total collection of resting-state networks is stronger than the SC supporting the collective set of networks associated with the auditory processing task. Some of the identified networks from the auditory task, e.g. the visual network, are strongly connected, but several others exhibit weak DTT-based SC. The resting-state networks have at least moderate SC for a larger number of clusters.

DTI and associated DTT algorithms both have known limitations, including handling of non-Gaussian diffusion, crossing fibers, noise-related errors, and partial volume effects, among others (Mori and van Zijl, 2002). However, comparative assessments between DTT and *in vivo* studies in macaques, post mortem dissections in humans, histological architectures in rats, and experimental phantoms have revealed broad similarities between DTT and known underlying neuroanatomy (Croxson et al., 2005; Jellison et al., 2004; Lawes et al., 2008; Leergaard et al., 2010). The limitations of DTI and DTT may give rise to either false positive or false negative structural links in our awFC approach. The false negative (or erroneously missing) connections fail to draw strength from the underlying SC but should not otherwise introduce structural-related bias as the results will tend toward standard unweighted clustering. False positive results, on the other hand, could potentially introduce bias. Our method includes protective factors to mitigate the chance of such bias.

False positive connections due to the DTT algorithms are most likely to occur for very proximal regions. We conducted an empirical investigation (not reported above) to determine the probability of false positive fiber tracking results (by chance) between nearby voxels, under assumptions mirroring the FSL tractography algorithm, except assuming isotropic movement on a 3-D lattice. The probability that a stream leaving a voxel randomly passes through another voxel that is two steps away (diagonal moves are permissible in one step) is rather small (less than 0.008), and this probability diminishes for more distant relationships. By defining our whole-brain analysis on a regional level, where the regions are less proximal than neighboring voxels, the chance of the distance-related bias is even further mitigated. Nonetheless, we secondly implement a distance correction using a Poisson regression model for the connecting streams between regions, modeled as a function of the physical distance between the regions. We have demonstrated that awFC produces more strongly autocorrelated FC networks for our experimental data, relative to conventional unweighted clustering, even in light of the aforementioned limitations. As DTI and DTT approaches continue to advance, they can be incorporated into our analysis and should yield even higher accuracy for our awFC method.

Supplementary Material

Refer to Web version on PubMed Central for supplementary material.

Acknowledgments

References

Balslev D, Nielsen FA, Frutiger SA, Sidtis JJ, Christiansen TB, Svarer C, Strother SC, Rottenberg DA, Hansen LK, Paulson OB, Law I. Cluster analysis of activity-time series in motor learning. Human Brain Mapping. 2002; 15:135–145. [PubMed: 11835604]

Baumgartner R, Ryner L, Richter W, Summers R, Jarmasz M, Somorjai R. Comparison of two exploratory data analysis methods for fMRI: fuzzy clustering vs. principal component analysis. Magnetic Resonance Imaging. 2000; 18:89–94. [PubMed: 10642106]

Bowman FD, Patel R. Identifying Spatial Relationships in Neural Processing Using a Multiple Classification Approach. NeuroImage. 2004; 23:260–268. [PubMed: 15325373]

Bowman FD, Patel R, Lu C. Methods for detecting functional classifications in neuroimaging data. Human Brain Mapping. 2004; 23:109–119. [PubMed: 15340933]

Buckner RL, Andrews-Hanna JR, Schacter DL. The Brain's Default Network: Anatomy, Function, and Relevance to Disease. Ann NY Acad Sci. 2008; 1124(1):1–38. [PubMed: 18400922]

Behrens TEJ, Woolrich MW, Jenkinson M, Johansen-Berg H, Nunes RG, Clare S, Matthews PM, Brady JM, Smith SM. Characterization and Propagation of Uncertainty in Diffusion-Weighted MR Imaging. Mag Res in Med. 2003; 50:1077–1088.

Behrens TEJ, Johansen-Berg H, Jbabdi S, Rushworth MFS, Woolrich MW. Probabilistic diffusion tractography with multiple fibre orientations: What can we gain? NeuroImage. 2007; 34:144–155. [PubMed: 17070705]

Cavanna AE, Trimble MR. The precuneus: a review of its functional anatomy and behavioural correlates. Brain. 2006; 129:564–583. [PubMed: 16399806]

Cordes D, Haughton V, Carew J, Arfanakis K, Maravilla K. Hierchical clustering to measure connectivity in fMRI resting-state data. MRI. 2002; 20:305–317.

Craddock RC, James GA, Holtzheimer PE III, Hu XP, Mayberg HS. A whole brain fMRI atlas generated via spatially constrained spectral clustering. Human Brain Mapping. 201110.1002/hbm. 21333

Croxson PL, Johansen-Berg H, Behrens TEJ, Robson MD, Pinsk MA, Gross CG, Richter W, Richter MC, Kastner S, Rushworth MFS. Quantitative Investigation of Connections of the Prefrontal Cortex in the Human and Macaque using Probabilistic Diffusion Tractography. J Neurosci. 2005; 25:8854–8866. [PubMed: 16192375]

Derado G, Bowman FD, Ely T, Kilts C. Evaluating Functional Autocorrelation within Spatially Distributed Neural Processing Clusters. Statistics and Its Interface. 2010; 3:45–57. [PubMed: 21643436]

Duda, RO.; Hart, PE. Pattern classification and scene analysis. New York: John Wiley and Sons; 1973.

Fadili MJ, Ruan S, Bloyet D, Mazoyer B. On the number of clusters and the fuzziness index for unsupervised FCA application to BOLD fMRI time series. Med Image Anal. 2001; 5:55–67. [PubMed: 11231177]

Fink GR, Markowitsch HJ, Reinkemeier M, Bruckbauer T, Kessler J, Heiss WD. Cerebral representation of one's own past: Neural networks involved in autobiographical memory. Journal of Neuroscience. 1996; 16(13):4275–4282. [PubMed: 8753888]

Friston KJ, Frith C, Liddle P, Frackowiak RSJ. Functional connectivity: The principal component analysis of large data sets. J Cereb Blood Flow Metab. 1993; 13:5–14. [PubMed: 8417010]

Fox MD, Snyder AZ, Vincent JL, Corbetta M, Van Essen DC, Raichle ME. The human brain is intrinsically organized into dynamic, anticorrelated functional networks. PNAS. 2005; 102(27): 9673–9678. [PubMed: 15976020]

Goutte C, Nielsen FÅ, Liptrot MG, Hansen LK. Feature-space clustering for fMRI meta-analysis. Human Brain Mapping. 2001; 13(3):165–183. [PubMed: 11376501]

Greicius MD, Supekar K, Menon V, Dougherty RF. Resting-State Functional Connectivity Reflects Structural Connectivity in the Default Mode Network. Cerebral Cortex. 2009; 19(1):72–78. [PubMed: 18403396]

Honey CJ, Sporns O, Cammoun L, Gigandet X, Thiran JP, Meuli R, Hagmann P. Predicting human resting-state functional connectivity from structural connectivity. PNAS. 2008; 106(6):2035–2040. [PubMed: 19188601]

Jellison BJ, Field AS, Medow J, Lazar M, Salamat MS, Alexander AL. Diffusion tensor imaging of cerebral white matter: A pictorial review of physics, fiber tract anatomy and tumor imaging patterns. Am J Neuroradiol. 2004; 25:356–369. [PubMed: 15037456]

Jenkinson M, Bannister P, Brady M, Smith S. Improved optimisation for the robust and accurate linear registration and motion correction of brain images. NeuroImage. 2002; 17(2):825–841. [PubMed: 12377157]

Johnson MK, Raye CL, Mitchell KJ, Touryan SR, Greene EJ, Nolen-Hoeksema S. Dissociating medial frontal and posterior cingulate activity during self-reflection. Soc Cogn Affect Neurosci. 2006; 1(1):56–64. [PubMed: 18574518]

Lawes IN, Barrick TR, Murugam V, Spierings N, Evans DR, Song M, Clark CA. Atlas-based segmentation of white matter tracts of the human brain using diffusion tensor tractography and comparison with classical dissection. NeuroImage. 2008; 39(1):62–79. [PubMed: 17919935]

Lazar M, Alexander A. Bootstrap white matter tractography (BOOT-TRAC). NeuroImage. 2005; 24:524–532. [PubMed: 15627594]

Leergaard TB, White NS, de Crespigny A, Bolstad I, D'Arceuil H, et al. Quantitative Histological Validation of Diffusion MRI Fiber Orientation Distributions in the Rat Brain. PLoS ONE. 2010; 5(1):e8595.10.1371/journal.pone.0008595 [PubMed: 20062822]

Ling J, Merideth F, Caprihan A, Pena A, Teshiba T, Mayer AR. Head injury or head motion? Assessment and quantification of motion artifacts in diffusion tensor imaging studies. Human Brain Mapping. 2012; 33:50–62. [PubMed: 21391258]

Maddock RJ. The retrosplenial cortex and emotion: New insights from functional neuroimaging of the human brain. Trends in Neurosciences. 1999; 22(7):310–316. [PubMed: 10370255]

Mayer AR, Mannell MV, Ling J, Elgie R, Gasparovic C, Phillips JP, Doezema D, Yeo RA. Auditory orienting and inhibition of return in mild traumatic brain injury: a fMRI study. Human Brain Mapping. 2009; 30:4152–4166. [PubMed: 19554558]

Morgan VL, Mishra A, Newton AT, Gore JC, Ding Z. Integrating Functional and Diffusion Magnetic Resonance Imaging for Analysis of Structure-Function Relationship in the Human Language Network. PLoS ONE. 2009; 4(8):e6660. [PubMed: 19684850]

Mori S, van Zijl PC. Fiber tracking: principles and strategies - a technical review. NMR in Biomedicine. 2002; 15:468–80. [PubMed: 12489096]

Parker G, Haroon H, Wheeler-Kingshott C. A Framework for a Streamline-Based Probabilistic Index of Connectivity (PICo) Using a Structural Interpretation of MRI Diffusion Measurements. Journal of Magnetic Resonance Imaging. 2003; 18:242–254. [PubMed: 12884338]

Rykhlevskaia E, Gratton G, Fabiani M. Combining structural and functional neuroimaging data for studying brain connectivity: A review. Psychophysiology. 2008; 45:173–187. [PubMed: 17995910]

Skudlarski P, Jagannathan K, Calhoun VD, Hampson M, Skudlarska BA, Pearlson G. Measuring Brain Connectivity: Diffusion Tensor Imaging Validates Resting State Temporal Correlations, NeuroImage. 2008; 43(3):554–561.

Smith S. Fast Robust Automated Brain Extraction. Human Brain Mapping. 2002; 17(3):143–155. [PubMed: 12391568]

Stanberry L, Nandy R, Cordes D. Cluster analysis of fMRI data using dendrogram sharpening. Human Brain Mapping. 2003; 20:201–219. [PubMed: 14673804]

Tzourio-Mazoyer N, Landeau B, Papathanassiou D, Crivello F, Etard O, Delcroix N, Mazoyer B, Joliot M. Automated anatomical labeling of activations in SPM using a macroscopic anatomical parcellation of the MNI MRI single-subject brain. NeuroImage. 2002; 15:273–289. [PubMed: 11771995]

van den Heuvel MP, Mandl RCW, Kahn RS, Hulshoff Pol HE. Functionally Linked Resting-State Networks Reflect the Underlying Structural Connectivity Architecture of the Human Brain. Human Brain Mapping. 2009; 30:3127–3141. [PubMed: 19235882]

Wang K, Jiang T, Yu C, Tian L, Li J, Liu Y, Zhou Y, Xu L, Song M, Li K. Spontaneous Activity Associated with Primary Visual Cortex: A Resting-State fMRI Study. Cerebral Cortex. 2008; 18:697–704. [PubMed: 17602140]

APPENDIX: Simulation Model

We generate both functional and structural distances, separately for within-network (indexed by $r=1$) and cross-network (indexed by $r=0$) region pairs, to conduct our simulation studies. Based on our experimental resting state fMRI and DTT data, the functional and structural distances are well-approximated by a normal distribution and a gamma distribution, respectively. Additionally, correlations exist between the functional and structural distances. We use these properties to simulate data from the following joint hierarchical probability model (we drop the subscripts ij denoting region pairs, for simplicity):

$$[f_r|\pi_r, c] \sim Normal\left(\mu_r + \frac{\tau_r}{\sigma_{sr}^2}(\pi_r - \theta_r), c\left(\sigma_{fr}^2 - \frac{\tau_r^2}{\sigma_{sr}^2}\right)\right)$$
$$[\pi_r] \sim Gamma\left(\frac{\theta_r^2}{\sigma_{sr}^2}, \frac{\theta_{sr}^2}{\sigma_r}\right)$$

Specifically, we draw the SC probabilities π_r from a gamma distribution, where θ_r and σ_{sr}^2 are the mean and the variance, respectively. Conditional on π_r, we draw the functional distances from a normal distribution. The conditional specification builds in correlations between the functional and structural distances, and τ_r is the covariance between these measures. The quantity c is a scale factor that we use to inflate the variances of the functional distances. We assess the impact of noise by setting $c=1,2$, and 3. We use estimates from our experimental data to set the values of the simulation parameters. The simulated data are very representative of the experimental data.
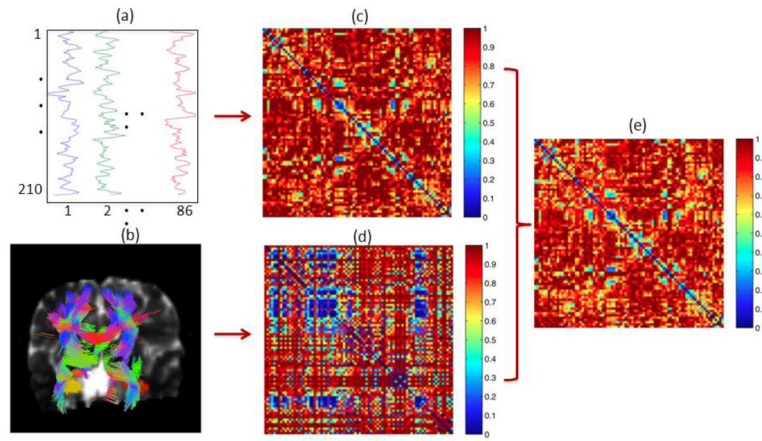
Figure 1.
Overview of preclustering steps in the awFC approach. (a) Regional fMRI profiles of resting state brain activity. (b) Diffusion tensor tractography results (we compute region-to-region probabilities of SC). (c) Functional distances between fMRI signals in (a). (d). Structural distances computed from SC probabilities. (e) Anatomically-weighted functional distances calculated by combining information from (c) and (d) as specified in equation (2).
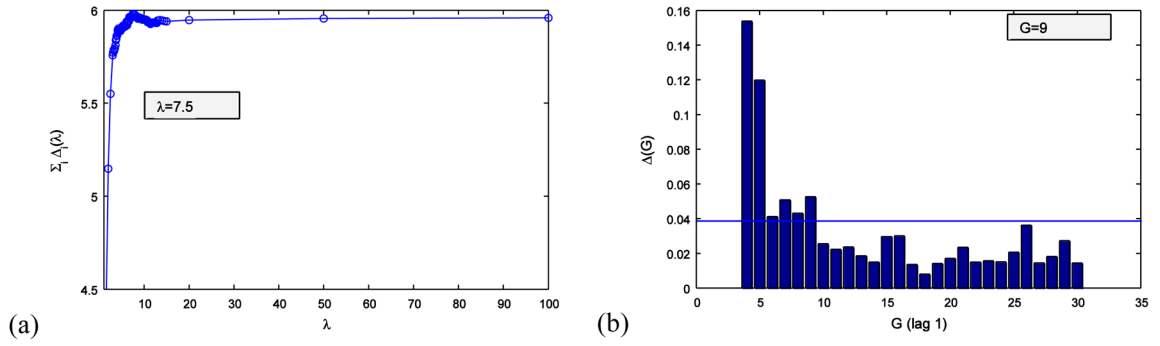
Figure 2.
Optimization results for a selected subject (subject 1) from the awFC method applied to the resting-state fMRI data. (a) Marginal summary of the optimization function with respect to λ. Our method identifies $\lambda = 7.5$ as the optimal value for our resting-state fMRI data. (b) Marginal summary of the optimization function with respect to G. The plot reveals large improvements in the clustering solutions with sequential increases in G at small values, but relatively little improvement beyond 9 clusters.
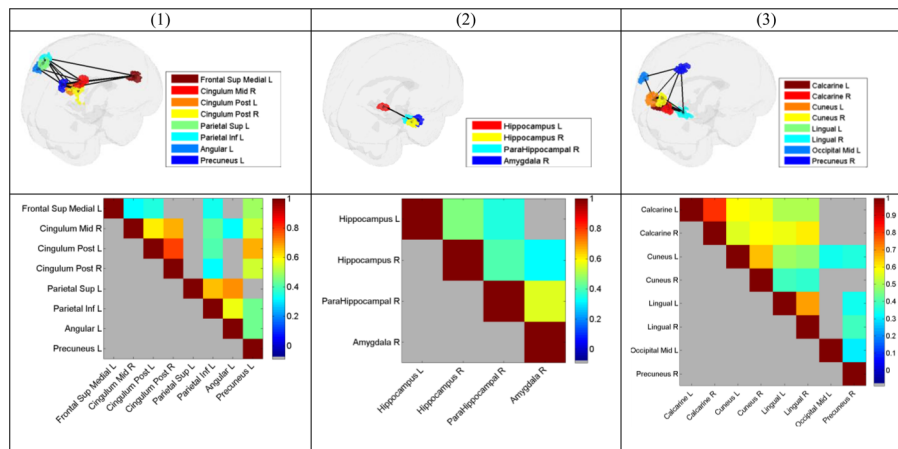
Figure 3.
Group-level resting-state networks. Cluster 1 consists of the left medial frontal gyrus, left and right posterior cingulate, left inferior parietal region, left angular gyrus, and left precuneus. This network reflects the integration of executive functioning, experiential self-reflection, and sensory perception and interpretation. Cluster 2 is a memory network and consists of medial temporal lobe regions including left and right hippocampus and right parahippocampal gyrus. Cluster 3 is a visual network that contains the left middle occipital gyrus. The line segments and the plots of matrices reflect region pairs with correlations that are statistically significantly greater than 0.25 (α=0.10 familywise error rate).
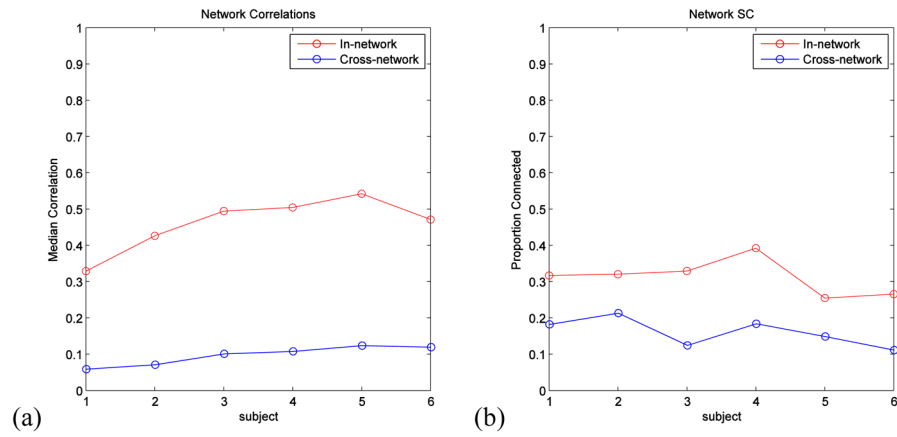
Figure 4.
(a) Within-network (red) and cross-network (blue) median FC for each subject. (b) Proportion of region pairs exhibiting SC, defined as Pr(SC) 0.5, within-network (red) and cross-network (blue) for each subject. The in- versus cross-network differences are all statistically significant. The network structure identified by our anatomically-weighted clustering technique reflects increased FC and SC for each subject.
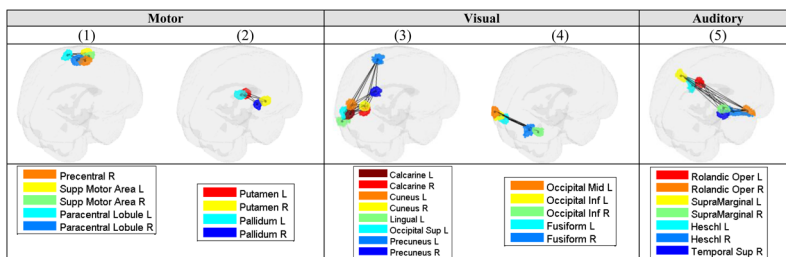
Figure 5.
Group-level functional networks identified from awFC for the auditory processing fMRI data. Seven clusters largely capture motor, visual, and auditory processing involved in the task. The line segments reflect region pairs with correlations that are statistically significantly greater than 0.25 (α=0.10 familywise error rate).

(a)

(b)
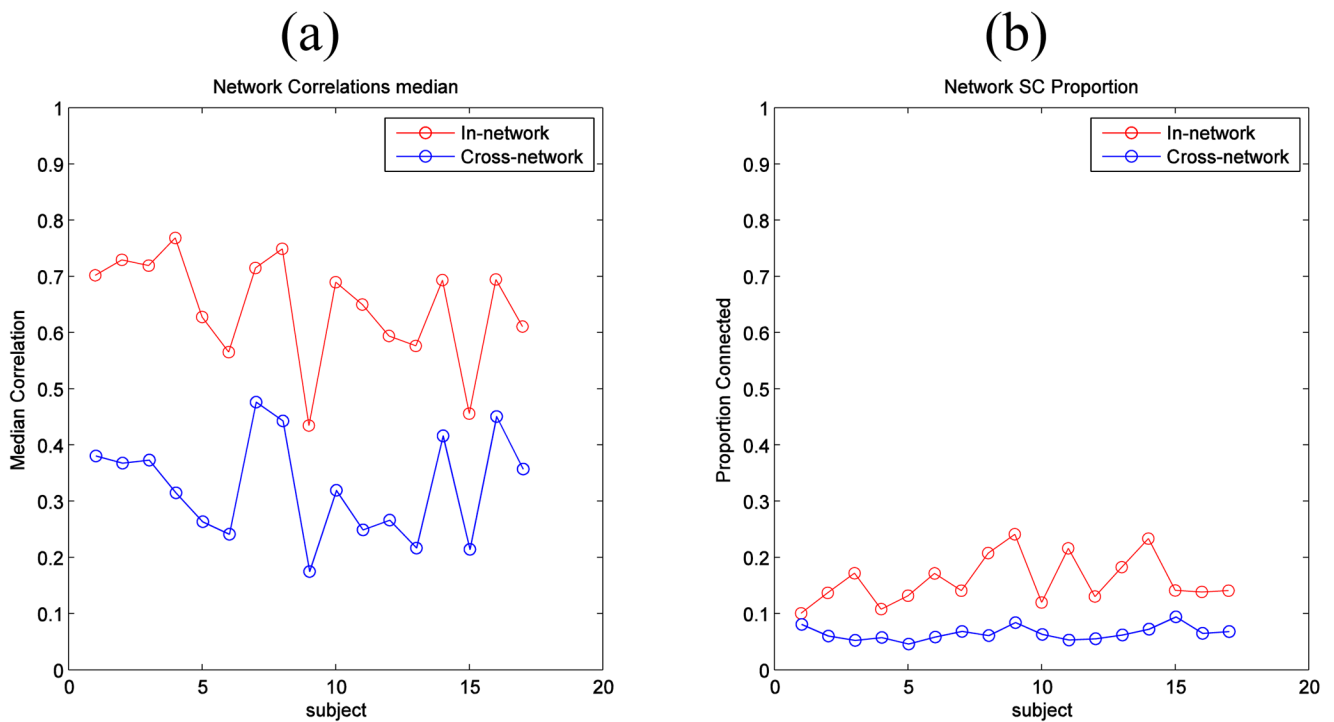
Figure 6.
(a) Within-network (red) and cross-network (blue) median FC for each subject. (b) Proportion of region pairs exhibiting SC, both within-network (red) and cross-network (blue) for each subject. The in-network FC versus cross-network FC differences are all statistically significant at $p{<}0.0001$. The in-network SC versus cross-network SC differences are statistically significant at $p{<}0.006$ for 16 of the 17 subjects.

Table 1

Simulation results comparing awFC to unweighted clustering. Values represent percent accuracies and standard errors (in parentheses). G=13 clusters, and σ^2 set using the experimental DTI and resting-state fMRI data.

Noise-level	Accuracy	awFC (λ=7.5) % (s. e.)
σ^2	Overall	99.35 (0.60)
	In-network	98.07 (2.01)
	Cross-network	99.55 (0.46)
$2\sigma^2$	Overall	97.32 (1.26)
	In-network	91.17 (4.73)
	Cross-network	98.31 (0.88)
$3\sigma^2$	Overall	95.10 (1.72)
	In-network	82.79 (6.84)
	Cross-network	97.09 (1.12)

$\sigma^2 = \left(\sigma_f^2 - \tau^2/\sigma_s^2\right)$, where σ_f^2 is the variance of the functional distances, σ_s^2 is the variance of the structural distances, and τ^2 is the covariance between the functional and structural distances.